RSC Advances

ROYAL SOCIETY OF CHEMISTRY

www.rsc.org/advances

For Table of contents entry

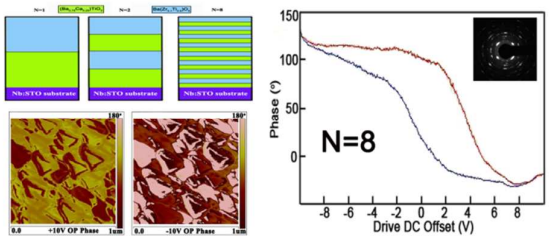

The piezo response is greatly strengthened by the interface effect and twining structures in $Ba(Zr,Ti)O_3/(Ba,Ca)TiO_3$ multilayered heterostructures.

RSC Advances

ARTICLE

Ferroelectric Domain Structure Evolution in $Ba(Zr_{0.1}Ti_{0.9})O_3/(Ba_{0.75}Ca_{0.25})TiO_3$ Heterostructures

Xiao Na Zhu,[a,b] Xing Xu,[b] Zach Harrell,[b] Ruyan Guo,[c] Amar S. Bhalla,[c] Minghui Zhang,[d] Jiechao Jiang,[d] Chonglin Chen,[b,†] Xiang Ming Chen[a,†]

Received 00th January 20xx,
Accepted 00th January 20xx

DOI: 10.1039/x0xx00000x

www.rsc.org/

Highly oriented multilayerd $Ba(Zr_{0.1}Ti_{0.9})O_3/(B_{a0.75}Ca_{0.25})TiO_3$ thin films were fabricated on Nb doped (001) $SrTiO_3$ (Nb:STO) substrates by pulsed laser deposition. Microstructural characterization by X-ray diffraction indicates that the as-deposited multilayered thin films are highly c-axis oriented. Transmission electron microscopy shows that the films present epitaxial correspondence with the substrate at the first layer and multi-oriented twin domain structures near the surface, especially with increasing periodic number (N). Piezoresponse force microscopy (PFM) studies reveal an intense polarization component in the out-of-plane direction, which increases greatly with increasing periodic number (N), whereas the in-plane shows inferior phase contrast. The optimized combination was found to be the annealed 16 layer structure (N=8, layer thickness = 712 nm) which displays the best polarization domain structures and the saturated piezo response loop. The annealing process benefits the 180° domains with some angle to the growth direction, which brings more piezo response in the in-plane signal. Our results suggest that the increasing of piezo response is greatly associated with interface effect and the twining structure.

Introduction

Perovskite ferroelectric materials are the most popular candidates for electronic devices, such as pluralized capacitors, actuators, sensors, etc.[1,2] Numerous investigations have been conducted on perovskite solid solutions formed with designed chemical elements for different industrial demands. $(Ba,Sr)TiO_3$ relaxor has been widely used in energy storage, microwave elements or capacitors.[3] $Pb(Zr_{1-x}Ti_x)O_3$ (PZT) is known more for its great piezoelectric performance, desired for the novel electromechanical devices. Later in this decade, research has shifted to searching for new alternatives to replace Pb-containing piezoeletronic materials due to toxity concerns.[4] Among all the Pb-free materials, alkaline niobate[5] and $BaTiO_3$ based[6-8] perovskites have been intensively explored due to their high d_{33} value. However, their d_{33} values remain inferior to Pb containing piezoelectric materials. Recently, a surprisingly high piezoelectric coefficient of d_{33}=620 pC/N in $Ba(Ti_{0.8}Zr_{0.2})O_3$-$(Ba_{0.7}Ca_{0.3})TiO_3$ (BZT-BCT) ceramic was reported.[9] The strong piezoelectric effect was related to the morphotropic phase boundary (MPB) at a tetragonal–cubic–rhombohedral triple point, where a very low energy barrier for polarization rotation and lattice distortion could be obtained. This result motivated further investigations in the whole BZT-BCT system.[10-15]

[a]*Laboratory of Dielectric Materials, Department of Materials Science and Engineering, Zhejiang University, Hangzhou 310027, China*
[b]*Department of Physics and Astronomy, University of Texas at San Antonio, Texas 78249, USA*
[c]*Department of Electrical and Computer Engineering, University of Texas at San Antonio, San Antonio, TX 78249, USA*
[d]*Department of Materials Science and Engineering, University of Texas at Arlington, Arlington, TX 76019, USA*
† Corresponding authors: Chonglin.Chen@utsa.edu & xmchen59@zju.edu.cn.

Electronic Supplementary Information (ESI) available:
(1) Figure S1 and S2: topography image, OP-PFM phase image, and IP-PFM phase images of domain structure of $Ba(Zr_{0.1}Ti_{0.9})O_3$ and $(Ba_{0.75}Ca_{0.25})TiO_3$ films.
(2) Figure S3 and S4: Out-of-plane and in-plane phase image when 10 V bias is applied to the $Ba(Zr_{0.1}Ti_{0.9})O_3$ and $(Ba_{0.75}Ca_{0.25})TiO_3$sample surface, respectively.
(3) Figure S5: Schematic representation of individual domain switching displayed in OP signal (top row), and IP (middle row) signals.
See DOI: 10.1039/x0xx00000x

Thin films of lead-free ferroelectric materials normally show a less than satisfactory piezoelectric response, but have been highly sought after for use in many micro actuators and sensors. The recent studies on BZT-BCT thin films were fabricated using spin-coating,[16] screen printing,[17] sol-gel,[18] chemical solution method,[19] and pulsed laser deposition.[11,20-22] Large d_{33} values over 100 pm/V,[23,24] and enhanced remnant polarization[21] of 37 μC/cm^2 has been achieved in 0.5BZT-0.5BCT homogeneous films. In contrast to numerous investigations on BZT-BCT homogeneous films, multi-layered structures consisting of single BZT and BCT layers have not been reported yet. In any ferroelectric multilayer systems, the interfaces present and the size of the individual layers play a crucial role in deciding upon final properties. With delicate controlling of periods of layer (N) or layer thickness, dielectric constant, tunability, or electromechanical properties can be enhanced greatly.[25-30] S. Zhong et al. theoretically reported a nearly 23% strain in $PbZr_xTi_{1-x}O_3$ multilayers.[27] Liu et al. reported five times larger microwave tunability in N=16 $BaTiO_3/SrTiO_3$ multilayer than that of N=4 multilayer.[28] R. Nath et al. revealed about 50 percent improvement of piezo response in $Ba_xSr_{1-x}TiO_3$ multilayered films than that of homogeneous samples.[29] The abundant physics mechanisms in multilayers triggered prosperous progress in microelectronic systems. Therefore, to introduce a multilayered structure into highly interesting BZT-BCT materials, using different periods of BZT and BCT single layer, is expected to achieve intriguing behaviours.

In this article, we have addressed the systematicl investigation of the relationship between the optimized microstructural combination and the enhanced piezo performance in the BZT-BCT multilayer system. We report here the multilayered $Ba(Zr_{0.1}Ti_{0.9})O_3/(Ba_{0.75}Ca_{0.25})TiO_3$ thin films deposited on single crystal Nb doped (001) $SrTiO_3$ substrate with different stacking layer numbers (N=1, 2 and 8), as seen in Figure 1. It is revealed that the piezo response is significantly dependent on the interface effect and the twining structure as the number of layers increase. The results are expected to provide a guideline on designing new structures for piezo materials in micro-electromechanical systems (MEMS).

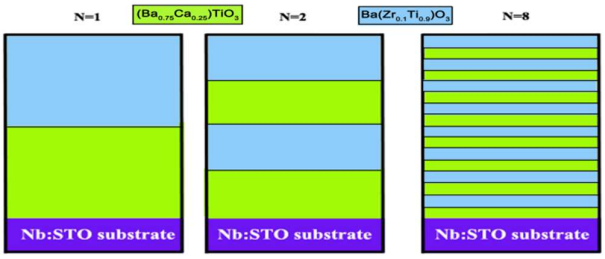

Figure 1. Sketch for the formula of BZT/BCT superlattices structure.

Experiments

A KrF excimer pulsed laser deposition system with a wavelength of 248 nm with the energy density of about 2 J/cm^2 and a repetition rate of 5 Hz was employed to fabricate ferroelectric BCT-BZT multilayered thin films on single-crystal (001) Nb:STO substrates. Single-phase pure $(Ba_{0.75}Ca_{0.25})TiO_3$ and $Ba(Zr_{0.10}Ti_{0.90})O_3$ targets were used for the deposition. The optimal growth conditions were found to be at the temperature of 840 °C with an oxygen pressure of 200 mTorr. The rate of the deposition time for the $(Ba_{0.75}Ca_{0.25})TiO_3$ and $Ba(Zr_{0.10}Ti_{0.90})O_3$ single-layer is 1:1 and the stacking periodic numbers are 1, 2, 8, respectively (as seen in Figure 1). The total deposition times were set to be 30 min with different stacking periodic combinations (N) to ensure the same total film thicknesses. For comparison, we also annealed a sample with N=8 at 450 ^{o}C in air for 24h to minimize the oxygen vacancy density in the film.

The microstructure, crystallinity, and epitaxial behavior of the as-deposited multilayered thin films were characterized by X-ray diffraction (XRD) and transmission electron microscopy (TEM). Cross-section TEM specimens were prepared via mechanical grinding, polishing and dimpling followed by Ar-ion milling. Selected-area electron diffraction patterns (SAED) and high-resolution TEM (HRTEM) images were recorded in a Hitachi H-9500 electron microscope (point resolution 0.18 nm). The PFM measurement was firstly characterized to achieve the topography, out of plane and in-plane images, with AC electric field added to the tip and the sample grounded. Then all the films were poled by scanning over a 5×5 μm^2 area under a DC bias of +10 V applied to the tip, followed by another scanning with an applied bias of -10 V, while the sample was kept grounded during the whole process. After that, the samples were again scanned at AC electric field to offset the DC bias influence. The phase hysteresis loops were achieved using a similar process with DC bias phase scanning.

Result and discussion

Figure 2(a-d) shows the typical θ-2θ scans of the as-deposited BZT/BCT multilayered thin films on the Nb:STO substrates with different stacking periodic combinations (N). (00l) peaks appear in the θ-2θ scans for both the thin films and the substrates, indicating that the multilayered thin films have highly c-axis texture growth, or c-axis normal to the substrate surfaces. Two additional peaks around 31^o and 55^o can be observed, which correspond to (011) and (112) planes, respectively (according to $BaTiO_3$ phase, PDF 05-0626). With increasing stacking number N, the (112) peak becomes stronger, indicating that the film has preferred growth to align along the (112) direction, probably due to the twinning growth mechanism.[31,32] The full width at half maximum (FWHM) of the rocking curve around (002) peak is 0.075, 0.084 for N=1 and N=2 films, respectively. As stacking number N reaches 8, the FWHM is 0.065 and it becomes 0.126 after annealing. Figure 2(e-h) display the enlarged view from 2θ=40~50^o, inserted with ϕ scan taken along <101> direction for each sample. The satellite peaks around (002) reflections become visible with the increase of the combination numbers (N), suggesting good interface structures and strong interface effects. The sample of as-deposited N=8 shows at least three satellite peaks at 2θ≈43.93, 2θ≈44.46, and 2θ≈45.5. Therefore, the multilayer thickness can be estimated from these satellite peaks using the standard formula $L = [\lambda/(\sin\theta_{n+1}-\sin\theta_n)]$, where λCu(Kα) is the wavelength of the Cu(Kα) radiation and n corresponds to the nth satellite peak. Specifically, the thickness of every periodic layer (L) of the sample N=8 was found to be about 38.5 nm, giving the overall multilayer thickness of about 616 nm. The annealed N=8 sample does not show the clear satellite peaks, suggesting the partial elimination of the interfaces by annealing.

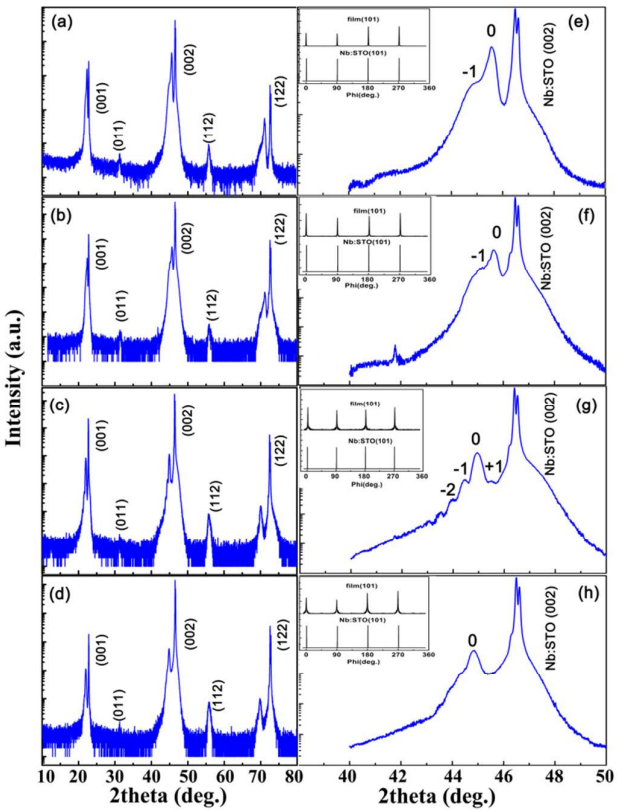

Figure 2. A typical X-ray diffraction pattern of the as-grown BZT/BCT multilayered thin films on (001) Nb:STO substrates for stacking number (a)N=1, (b) N=2 (c)N=8, (d)N=8 with post annealing for 24 hour at 450 °C, respectively. The second row (e-h) shows the broadened view from 2θ=40~50° for stacking number (e)N=1, (f) N=2 (g)N=8and (h)N=8 with post annealing for 24 hour at 450 °C, respectively, inserted with ϕ-scan taken along <101> for each sample.

We have conducted cross-sectional TEM studies to further understand the microstructure of the multilayered thin films. Figure 3(a) shows a bright-field TEM image of a 2 layer film (N=1). The thickness of BZT and BCT layer is about 280 nm and 160 nm, respectively. The growth rate of BCT layer was determined to be 10.0 nm/min, while that of BZT is about 20 nm/min. Clear and distinguished sharp interfaces between the BCT layer with respect to the STO substrate, and to the BZT layer were formed. Figure 3(e) is a SAED pattern taken from an interface region covering the Nb:STO substrate and the 1st layer of BCT, indicating a good epitaxial structure of the BCT layer was formed on the Nb:STO substrate. Figure 3(f) is a SAED pattern taken from the BZT layer in Figure 3(a) presenting a polycrystalline structure formed in the layer. The high intensity diffraction arcs around the (011) spot in the first diffraction ring in Figure 3(f) indicate the formation of some twin structures. These arcs could be also observed in the epitaxial BZT and Mn:BZT structures.[31,32]

Figure 3(b) shows a TEM image of 4 layer film (N=2). The total thickness of the BZT and BCT layer is about 650 nm, which is surprisingly thicker than what was designed. The 1st layer of BCT appears much darker than the three layers above. The SAED pattern taken from the 1st BCT layer/STO substrate exhibits the same characteristics as shown in Figure 3(e), indicating an epitaxial structure with respect to the STO substrate. The top three layers in Figure 3(b) present a columnar structure. Figure 3(g) is a SAED pattern taken from the top three layers, exhibiting polycrystalline structure. Formation of such polycrystalline structures may be associated with the high deposition rate.

Figures 3(c) and (d) are cross-sectional TEM images of the as-deposited and annealed 16 layer films (N=8). The multilayered structure is clearly shown in the as-deposited film but can be barely seen in the post annealed film. The annealed film shows better defined columnar structures than the as-deposited film. Similar to the aforementioned films, the 1st BCT layer appears much darker contrast than the layers on its top. Electron diffraction analysis shows that the 1st BCT layer in both as-deposited and annealed films possesses an epitaxial structure. Figures 3(h) and (i) are SAED patterns taken from the layers on the top of the 1st BCT layer. Figure 3(h) presents mainly the (011) and (01$\bar{1}$) diffractions. It is significantly different from the SAED patterns shown in Figure 3(f) and (g). This result indicates that this as-deposited N=8 film mainly consists of twin structures that are formed by coherently joining their {111} planes.[31,32] Figure 3(i) shows that in addition to the strong (011) and (01$\bar{1}$) diffraction spots, the intensity of the other diffraction rings are significantly increased. This indicates that the twin structures in the as-deposited film are degraded during the annealing. However, the annealed film still possesses a significant amount of twin structures.

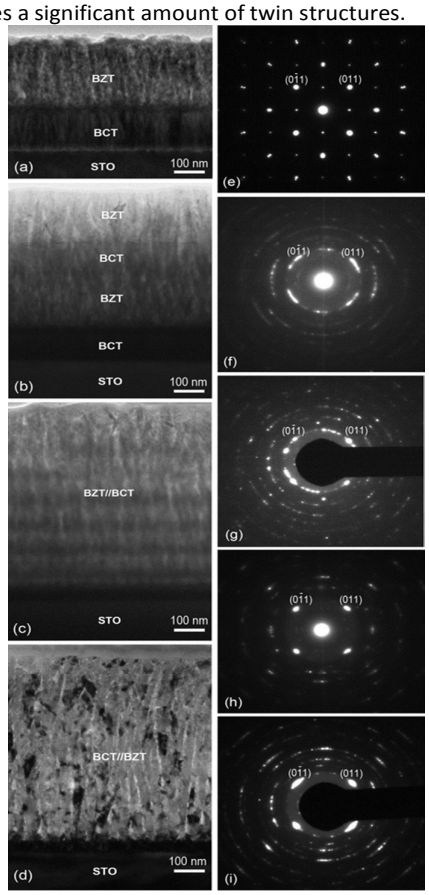

Figure 3. Cross-sectional TEM images of as-grown BZT/BCT 2-layer (a), 4-layer (b), 16-layer (c), and of post annealed BZT/BCT 16 layer (d) film. (e) SAED pattern taken from the interface covering 1st layer BCT and Nb:STO substrate. (f)-(i) SAED pattern taken from the region above

the first BCT layer in the as-grown BZT/BCT 2-layer, 4-layer, 16-layer, and post annealed BZT/BCT 16 layer film, respectively.

It can be summarized from the aforementioned results that the 1st BCT layer is epitaxially grown on the (001) Nb:STO substrate in the four films studied in the paper. Figure 4 shows a typical cross-section HRTEM image of such an interface between the 1st BCT layer and the Nb:STO substrate. It clearly shows that the BCT layer is very well epitaxially grown on the STO substrate with an atomically sharp interface with respect to the substrate.

Figure 5(a) is a HRTEM image of an interface between the 1st BCT layer and the BZT layer taken from the 4 layer film. It can be seen that the BZT structure was initially epitaxially grown on the 1st BCT layer. However with the further growth of the BZT layer, the front surface of the BZT layer starts to become rough and in the meantime the twin structures formed by coherently joining their {111} planes with the epitaxial structure were developed.

Figure 5(b) is a HRTEM image taken from the film region above the 1st BCT layer in the as-grown 16 layer film showing the coexistence of several twin domain structures, such as Twin 1 and Twin 2. The following PFM results show that the films composed of such twin structures exhibit significantly enhanced properties.

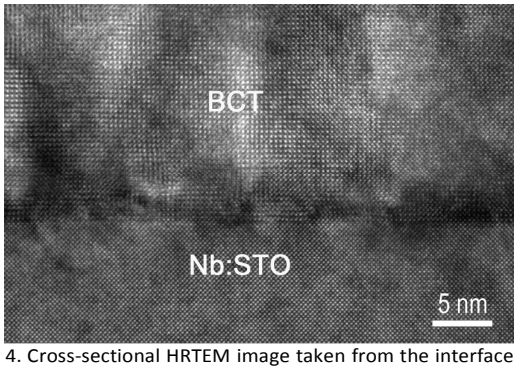

Figure 4. Cross-sectional HRTEM image taken from the interface of 1st BCT layer and Nb:STO substrate.

To understand the dielectric properties of the as-grown films, PFM was used to investigate the piezo response features of both out-of-plane (OP-PFM) and in-plane (IP-PFM) phase images. Figure 6(a) shows the surface topography of all the films with different stacking numbers. As seen in Figure 6(a), all samples have a flat surface. The sample with N=1 shows a round grain shape while samples with N=2 and N=8 show triangular shaped dense blocks. These surface structures manifest a clear texture of triangular pyramid and stair-step shapes. This triangular shape morphology was also reported in previous reports on BZT-BCT thin films.[25,33] The average grain size calculated by linear intercept method is 124 nm, 294 nm, and 250 nm, for the as-deposited films of N=1, N=2, and N=8, respectively. The grain size gradually increases with the stacking periodic number increasing. It is worth noting that $(Ba_{0.75}Ca_{0.25})TiO_3$ terminated film has a smaller grain size than the $Ba(Ti0_{.9}Zr_{0.1})O_3$ terminated film (see Figure S1 and S2(a)), suggesting that BZT needs more nucleation energy to form grains. This is due to slow diffusion of bigger Zr^{4+} ions replacing smaller Ti^{4+} ions at B sites of oxygen octahedra. Thus, the BZT layer has smaller interface energy due to larger grain size and less grain boundaries.

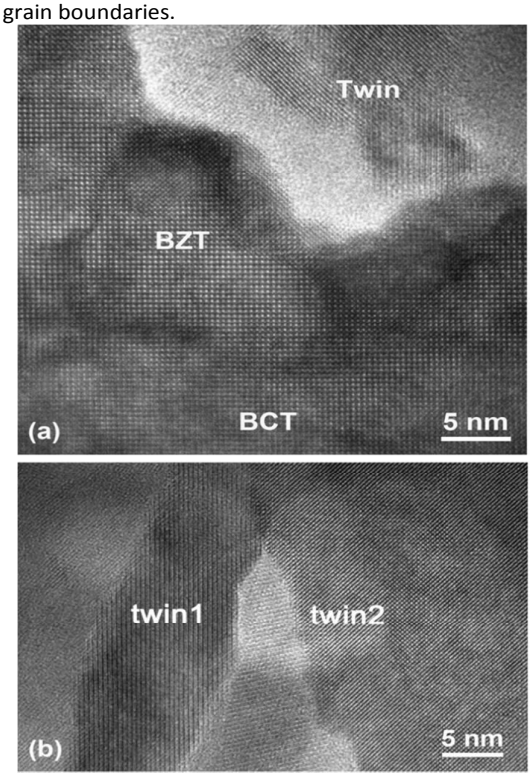

Figure 5. (a) cross-sectional HRTEM image of the interface between 1st BCT layer and BZT layer. (b) a typical HRTEM image taken from a region above 1st BCT layer in the as-grown BZT/BCT 16 layer thin film.

The representative out-of-plane (OP) and in plane (IP) PFM phase images are shown in Figure 6(b) & (c), respectively. As to the phase image, an AC bias voltage is applied between tip and sample during contact mode imaging. In response to the AC electric field, the sample expands and contracts, leading to an oscillation in cantilever deflection. Thus the color contrast actually means the deflection feedback of the cantilever due to the different poling state in the neighboring domains. The N=1 sample shows a 90^o contrast in OP phase image, while N=2 and N=8 samples show 180^o contrast. Thus, it suggests a stronger out-of-plane component of polarization with increasing layer number. As to the IP phase, all the samples show a relatively low contrast (45 or 25 degree). This indicates that the in-plane component of ferroelectric domain is smaller compared to the out-of-plane element. As it can be observed in Figure S1 and S2 (b) & (c), the BCT or BZT terminated film only shows 5 degrees in IP phase image, and 90 and 45 degree contrast in OP phase image, respectively. It can be compared that the piezo response of both OP and IP phases are getting stronger with increasing layer number, and the increase of OP phase contrast is larger than that of IP phase contrast. One reason for the increasing OP contrast is the twining structure exhibited with increasing layer number. According to the previous TEM discussion, the sample of N=1 is strained along (001) at the first BCT layer, and then relaxed to a polycrystal at the top of the BZT layer. In contrast, in the N=8 film, the top BZT layer remains highly textured growth along the (011) direction, joining their {111} planes. Compared to the (001) oriented layer, the (111) or (011) oriented layers bring

larger tetragonal lattice distortion, and also arouse a larger angle relationship between the film orientation and the spontaneous polarization.[23] This orientation dependent phenomenon is also quite consistent with lead-based films. The domain morphology in $Pb(In_{1/2}Nb_{1/2})O_3$-$Pb(Mg_{1/3}Nb_{2/3})O_3$ material is reported to largely depend on the crystal orientation. The (011) orientated crystal is inferred to have distinctive domain behaviour.[34] Similarly, the (011) twining structure here in the N=8 film is a key factor for the superior piezoelectric response. Another reason for the increasing OP contrast can be attributed to the strain enhancement of polarization. The strain introduced at the interface becomes much higher as the thickness of each individual layer decreases. Large amounts of theoretical analysis on the strain enhanced piezo responses have shed a light on this phenomenon. The mis-fit strain can largely control the out-of plane domain structure, reported in $Pb(Zr,Ti)O_3$ films.[35] Regarding that the BCT layer has a smaller lattice constant than that of the BZT layer, it suffers a tensile strain from the BZT layer, and vice versa, the BZT layer suffered a comprehensive strain. This periodic strain modulation behaves more evidently as the number of layers increase. In addition, since the increase of OP contrast is larger than that of IP contrast as number of layers increase, it can be inferred that the polarization direction is tending to form along the growth direction (z axis) as number of interfaces increase. In summary, the interface between BZT and BCT plays an important role in the enhancement of the piezo response performance.

In order to investigate the domain switching behaviours, a bias of 10 volt is added positively and negatively to the tip. Figure 7 displays the OP phase image and IP phase image when (a), (c) +10 V and (b), (d) −10 V bias is applied to the sample surface, respectively. With periodic number (N) increasing, the OP contrast between positive (+10v) and negative (-10V) poled image increases greatly (see Figure 7(a)&(b)). The sample of as-deposited N=8 (see Figure 7 (III) (a) & (b)) shows best switching behaviour in OP phase signal. In contrast, the BZT or BCT terminated film shows the weakest switching contrast (see Figure S3 and S4). As more interfaces are induced into films, better switching can be achieved. In addition, the IP phase signal is not sensitive to the interfaces increasing compared to OP phase signal. However, the annealing sample displays a much stronger IP switching contrast, suggesting polarization component not strictly along z axis existed in the annealing sample.

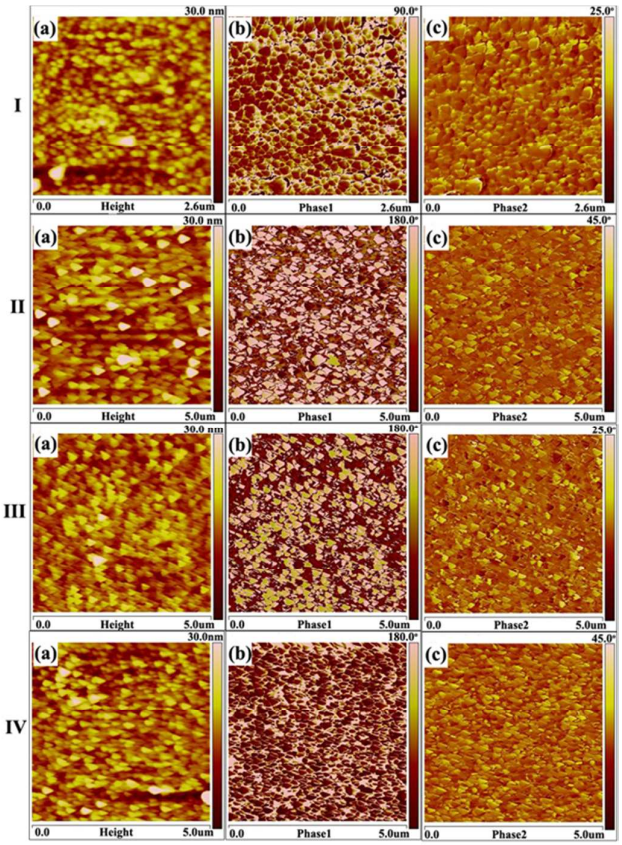

Figure 6. AFM images of BCT-BZT multilayered films with different stacking periodic numbers((I) N=1, (II) N=2, (III) N=8, and (IV) N=8 with post annealing) showing (a) contact mode topography image, (b) OP-PFM phase image, and (c) IP-PFM phase images of domain structure.

Since both OP and IP phase information has been recorded, it is possible to reconstruct the polarization direction into x-z plane.[36] The domain structure is classified into four categories in as deposited and annealed N=8 film. The schematic representation of the switching behaviour in these four types has been compared in Figure S5. It is difficult to distinguish 90^o domains and 180^o domains only according to the phase images in the x-z plane. However, as in the current work, we can basically rule out the existence of 90^o domains (type 3 and type 4), because they lead to strong changes in IP phase signal. This is similar to $Pb(Zr,Ti)O_3$ epitaxial films where (111) oriented films tend to form 180^o domains while relaxed films have many domains.[37] Therefore, we denoted the 180^o domain (type 1 and type 2) distribution in Figure 8 (marked as Red numbers). The as-deposited film of N=8 exhibits mainly type 1 domains, whereas the annealed sample of N=8 has a large amount of type 2 domains. This indicates that the annealing process changes the polarization direction in the N=8 films, giving more IP phase signal. In addition, it is interesting that different color contrast is observed at the domain boundary in annealed N=8 sample. Moreover, the domain boundary can be switched by DC electric field reversing. This behaviour is only observed in the annealed sample, which means the domain boundary has different polarization direction compared to the inner domain.

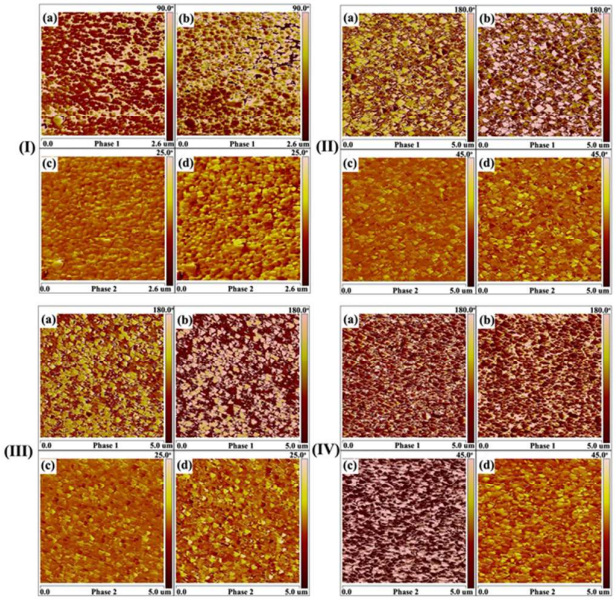

Figure 7. AFM images of BCT-BZT multilayered films with different stacking periodic numbers ((I) N=1, (II) N=2, (III) N=8, and (IV) N=8 with post annealing) showing: Out-of-plane phase image when (a) +10 V and (b) −10 V is applied to the sample surface, and in-plane phase image when (c) +10 V and (d) −10 V is applied to the sample surface, respectively.

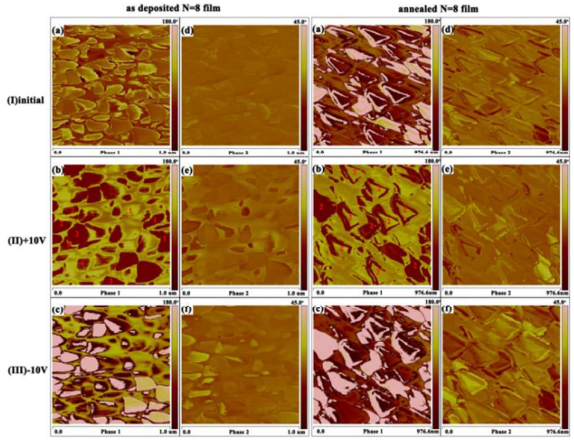

Figure 8. Switching behaviors of N=8 as deposited and post annealing films displayed in initial state (top row), +10V (middle row), and -10V (lower row) signals, showing: (a),(b),(c) Out-of-plane phase image, and (d),(e),(f) in-plane phase image.

Typical local piezo-loop measured at room temperature on a fixed location in the center of the BCT-BZT grain is shown in Figure 9. The sample of N=1 shows nearly 100° switching in OP phase, while the sample of N=2 shows 120° switching. The annealed N=8 sample can be reversibly switched 180°, qualitatively demonstrating complete ferroelectric polarization switching. Because all the amplitude and phase scanning used the same tip, we can set a laser sensitive coefficient of tip as a constant (unit: nm/V). The piezoelectric coefficients of all the films can be compared from the slope of the amplitude-voltage curves with positive linear portion. It can be compared that the sample of N=8 has a three times higher piezoelectric coefficient than the sample of N=1. This result coincides well with the former discussion of switching behaviour. The coercive voltage is found to be an average of 2.5V in all the samples. The switching is asymmetric with imprint behaviour as there is much difference between positive and negative coercive voltages.

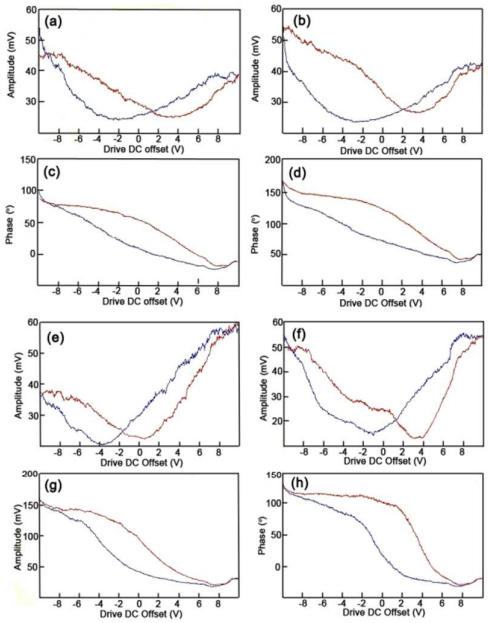

Figure 9. Amplitude hysteresis loop of BCT-BZT multilayered films of (a) N=1, (b) N=2, (e) N=8, and (f) N=8 with post annealing, and Phase hysteresis loop of BCT-BZT multilayered films of (c) N=1, (d) N=2, (g) N=8, and (h) N=8.

Conclusions

Multilayered $Ba(Zr_{0.1}Ti_{0.9})O_3/(Ba_{0.75}Ca_{0.25})TiO_3$ thin films deposited on Nb doped (001) $SrTiO_3$ substrates have a primary (001) orientation along the growth direction. XRD and TEM analysis reveals sharp interfaces and epitaxial nature at the BCT/Nb:STO interface, and multi-oriented twin domain structures formed near the surface as the number of layers increases. All films exhibit an intense polarization component in out-of-plane phase, and inferior in-plane phase contrast. As periodic number (N) increases, the out-of-plane phase contrast increases greatly and better switching behaviors are observed. The annealed N=8 sample shows the best polarization domain structures and saturated piezo response loop. Our results suggest that interface effects and the twining structure play an important role in enhancing the increase of piezo response.

Acknowledgements

This research was supported by the National Science Foundation under grant number of NSF-NIRT-0709293 and partially supported by National Natural Science Foundation of China under grant number 51332006.

References

1 A.K. Yadav, C.R. Gautam, Adv. Appl. Ceram., 2014, **113,** 193-207.
2 A.K. Yadav, C.R. Gautam, J Mater Sci: Mater Electron, 2014, **25**, 5165–5187.
3 A.K. Yadav, C.R. Gautam, P. Singha, RSC Adv., 2015, **5**, 2819-2826.
4 Official J. Eur. Union L 2003, **037**, 0019.
5 Y. Saito, H. Takao, T. Tani, T. Nonoyama, K. Takatori, T. Homma, T. Nagaya, M. Nakamura, Nature, 2004, **432**, 84-87.
6 X.B. Ren, Nature Mater., 2004, 3, 91.
7 Z. Yu, C. Ang, R. Guo, A.S. Bhalla, J. Appl. Phys., 2002, **92**, 1489.
8 Y. Guo, K. Suzuki, K. Nishizawa, T. Miki, K. Kato, J. Cryst. Growth, 2005, **284**, 190-196.
9 W. Liu, X. Ren, Phys. Rev. Lett., 2009, **103**, 257602.
10 D. Damjanovic, A. Biancoli, L. Batooli, A. Vahabzadeh, J. Trodahl, Appl. Phys. Lett., 2012, **100**, 192907.
11 F. Benabdallah, A. Simon, H. Khemakhem, C. Elissalde, M. Maglione, J. Appl. Phys., 2011, **109**, 124116.
12 A. Piorra, A. Petraru, H. Kohlstedt, M. Wuttig, E. Quandt, J. Appl. Phys., 2011, **109**, 104101.
13 V.S. Puli, A. Kumar, D.B. Chrisey, M. Tomozawa, J.F. Scott, R.S. Katiyar, J. Phys. D: Appl. Phys., 2011, **44**, 395403.
14 J. Gao, D. Xue, Y. Wang, D. Wang, L. Zhang, H. Wu, S. Guo, H. Bao, C. Zhou, W. Liu, S. Hou, G. Xiao, X. Ren, Appl. Phys. Lett., 2011, **99**, 092901.
15 D. Xue, Zhou, Y. H. Bao, C. Zhou, J. Gao, X. Ren, J. Appl. Phys., 2011, **109**, 054110.
16 Z. Wang, K. Zhao, X. Guo, W. Sun, H. Jiang, X. Han, X. Tao, Z. Cheng, H. Zhao, H. Kimura, G. Yuan, J. Yin, Z. Liu, J. Mater. Chem. C, 2013, **1**, 522.
17 W. Bai, B. Shen, F. Fu, J. Zhai, Mater. Lett., 2012, **83**, 20-22.
18 Y.T. Lin, G.H. Wu, N. Qin, D.H. Bao, Thin Sol. Films, 2012, **520**, 2800.
19 G.Q. Kang, K. Yao, J. Wang, J. Am. Ceram. Soc., 2012, **95**, 986.
20 C. Bhardwaj, B.S.S. Daniel, D. Kaur, J. Phys. Chem. Sol., 2013, **74**, 94-100.
21 Y.D. Kolekar, A. Bhaumik, P.A. Shaikh, C.V. Ramana, K. Ghosh, J. Appl. Phys., 2014, **115**, 154102.
22 Q. Lin, D. Wang, Li. S, J. Am. Ceram. Soc., 2015, 1-5.
23 Luo, B.C. Wang, D.Y. Duan, M.M. S. Li, Appl. Phys. Lett., 2013, **103**, 122903.
24 A. Jalalian, A.M. Grishin, X.L. Wang, Z.X. Cheng, S.X. Dou, Appl. Phys. Lett., 2014, **104**, 103112.
25 P.R. Choudhury, S.B. Krupanidhia, J. Appl. Phys., 2008, **104**, 114105.
26 H. Tabata, H. Tanaka, T. Kawai, Appl. Phys. Lett., 1994, **65**, 1970.
27 S. Zhong, Z.G. Ban, S.P. Alpay, J.V. Mantese, Appl. Phys. Lett., 2006, **89**, 142913.
28 M. Liu, C.R. Ma, G. Collins, J. Liu, C.L. Chen, C. Dai, Y. Lin, L. Shui, H. Wang, J. He, J.C. Jiang, E.I. Meletis, Q.Y. Zhang, M.W. Cole, ACS Appl. Mater. Interfaces, 2012, **4**, 5761.
29 R. Nath, S. Zhong, S.P. Alpay, B.D. Huey, M.W. Cole Appl. Phys. Lett., 2008, **92**, 012916.
30 M. Liu, J. Liu, C.R. Ma, G. Collins, C.L. Chen, A.D. Alemayehu, G. Subramanyam, J. He, J.C. Jiang, E.I. Meletis, A. Bhalla, Crys. Eng. Comm., 2013, **15**, 2267.
31 J. He, J.C. Jiang, E.I. Meletis, M. Liu, J. Liu, G. Collins, C.R. Ma, C.L. Chen, A. Bhalla, Phil. Mag. Lett., 2011, **91**, 361.
32 J. He, J.C. Jiang, E.I. Meletis, M. Liu, J. Liu, G. Collins, C.L. Chen, A. Bhalla, Phil. Mag. Lett., 2009, **89**, 493-503.
33 V.D.O. Doan, M.O. Lai, L. Lu, J. Phys. D: Appl. Phys., 2008, **41**, 205408.
34 Q. Li, Y. Liu, R.L. Withers, Y. Wan, Z. Li, Z. Xu, J. Appl. Phys., 2012, **112**, 052006.
35 Z. Jiang, R. Zhang, D. Wang, D. Sichuga, C.L. Jia, L. Bellaiche, Phys. Rev. B, 2014, **89**, 214113.
36 A. Roelofs, U. Böttger, R. Waser, F. Schlaphof, S. Trogisch, L.M. Eng, Appl. Phys. Lett., 2000, **77**, 3444.
37 R.L. Johnson-Wilke, D.S. Tinberg, C. Yeager, W.Qu, D.D. Fong, T.T. Fister, S.K. Streiffer, Y. Han, I.M. Reaney, S. Trolier-McKinstry, J. Appl. Phys., 2013, **114**, 164104.